Available online at www.sciencedirect.com

ScienceDirect

Energy Procedia 92 (2016) 218 – 224

Energy Procedia

6th International Conference on Silicon Photovoltaics, SiliconPV 2016

High resolution sheet resistance mapping to unveil edge effects in industrial IBC solar cells

Pierpaolo Spinelli[a]*, Pi Danzl[a], Nicolas Guillevin[a], Agnes Mewe[a], Simon Sawallich[b], Ard Vlooswijk[c], Bas van de Loo[d], Erwin Kessels[d], Michael Nagel[b], Ilkay Cesar[a]

[a]*Energy Research Centre of the Netherlands (ECN), Westerduinweg 3, 1755LE Petten, The Netherlands*
[b]*Protemics GmbH, Otto-Blumenthal-Str. 25, 52074 Aachen, Germany*
[c]*Tempress Systems B.V., Radeweg 31, 8171 MD Vaassen, The Netherlands*
[d]*Eindhoven University of Technology, P.O. Box 513, 5600 MB Eindhoven, The Netherlands*

Abstract

We present Terahertz (THz) transmission measurements with a spatial resolution of down to 10 µm as a new inspection technique for high-resolution sheet resistance (R_{sh}) measurements, that are well suited to quantify the local R_{sh} (n-type and p-type regions) of interdigitated back-contact (IBC) structures and to support further optimization of our IBC cells.
Using this technique, we investigated the homogeneity of the emitter of our IBC cells. We have greatly improved the R_{sh} homogeneity of the boron diffusion. Moreover, we compared THz mapping with standard four point probe (4pp) technique. While the 4pp measurement showed a homogeneous mapping, the THz could unveil elevated R_{sh} near the very edge of the wafer. Higher R_{sh} of the surface doping can result in higher J_0 at the metal contact regions ($J_{0,contact}$). A local V_{oc} mapping technique was used and it was found that the local V_{oc} at the wafer edge was lowered by 17 mV compared to the centre in the most extreme case. We estimate that an improved edge doping could result in a performance gain of at least 0.2% absolute, excluding FF and J_{sc} benefits.
In summary we show that THz mapping is a powerful method in determining inhomogeneities and can aid in the development of diffused-junction IBC solar cells.

Peer review by the scientific conference committee of SiliconPV 2016 under responsibility of PSE AG.

Keywords: IBC solar cells; sheet resistance; Terahertz transmission

* Corresponding author. Tel.: +31 885154697.
E-mail address: spinelli@ecn.nl

Peer review by the scientific conference committee of SiliconPV 2016 under responsibility of PSE AG.
doi:10.1016/j.egypro.2016.07.062

1. Mercury IBC cells at ECN

The Mercury cell developed at ECN is an IBC solar cell with a Front Floating Emitter (FFE). While IBC cell technology has been demonstrated ideal for high-efficiency solar cells [1] due to the absence of optical shading losses from front metallization, cost effective production of these devices is still challenging. The presence of electrical shading [2] limits the choice of back surface field (BSF) width to less than 0.4 mm, which in turn poses severe limitations on patterning and metallization tolerances.

The use of a FFE gives the IBC cell characteristics that are radically different from a front surface field (FSF) cells [3,4]. One main feature of the FFE is that it enables the so called "pumping effect" that creates a lateral flow of holes in the FFE from areas above the BSF to areas above the emitter. Holes are there re-injected into the base and collected by the rear emitter [5]. This overall has the effect of strongly mitigating electrical shading above the BSF compared to FSF cells. Because of the pumping effect, the BSF regions can be made wider than in FSF cells without sacrificing photocurrent. This allows lower resolution processing (e.g. standard screen printing), improves manufacturability and reduces the losses due to BSF busbars. In addition the FFE allows to widen the BSF area for busbar and pads for soldering tabs or interconnection to a conductive back sheet foil through a conductive adhesive. Figure 1 shows a schematic of the Mercury cell developed at ECN.

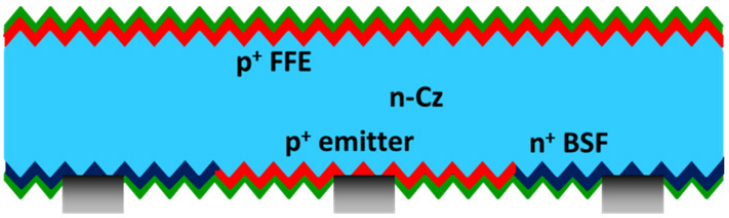

Fig. 1. Schematic of a Mercury IBC solar cell with FFE

Mercury cells of 156x156 mm^2 were processed at ECN on semi-square n-Cz wafers using the same process equipment as our industrial n-Pasha cell process [6]. Screen printed metallization was used and an isolation gap between rear emitter and BSF was omitted mainly for process simplicity. On 6-inch cells we obtained a best cell efficiency of 21.1% (full size illumination) as shown in Table 1.

Table 1. Best cell IV parameters for Mercury IBC solar cell

Area	J_{SC}	V_{OC}	FF	Efficiency
239 cm^2	41.2 mA/cm^2	653 mV	78.4%	21.1%

2. THz R_{sh} mapping method

Sheet resistance (R_{sh}) mapping is of great importance to characterize the homogeneity and doping levels of doped regions in solar cells. Usually four point probe (4pp) measurements are used to measure R_{sh}. However, this method lacks the resolution required for a detailed inspection of Interdigitated Back Contact (IBC) cells with sub-millimeter features.

THz transmission near-field imaging is a recently introduced inspection method for high-resolution large-area sheet resistance quantification [7]. Sheet resistance measurements with a high spatial resolution of a few µm are of general importance for the inspection of IBC cells in order to distinguish the fine patterning of the diffusions at the cell's rear side. Such measurements allow monitoring the accuracy of the patterning process, and help to avoid undesirable – and otherwise hardly detectable – local defects due to high contact resistance, or spiking through the diffusion during firing.

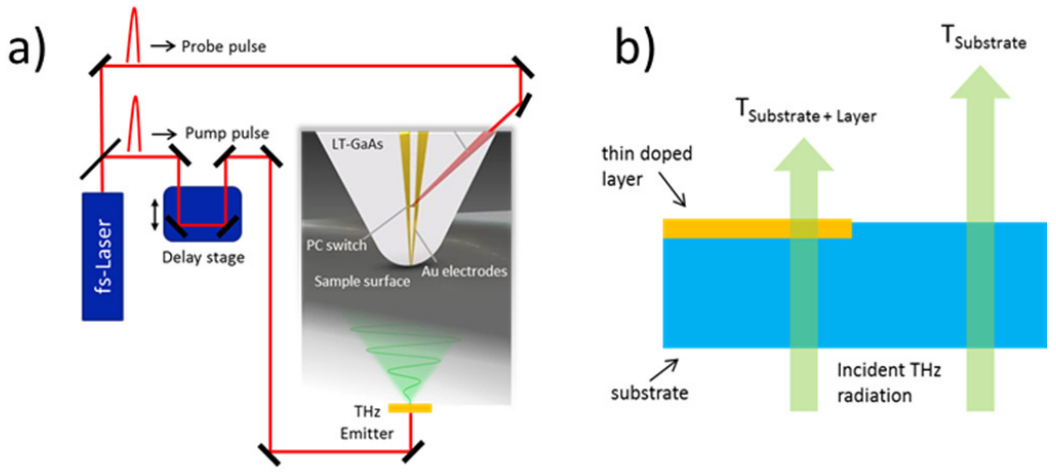

Fig. 2. a) Schematic of the THz near-field setup, and b) of the THz transmission amplitude reduction.

Measurements were performed in a THz transmission setup based on a pump/probe scheme, using broadband THz pulses. As described in an earlier publication [8], sub-wavelength spatial resolution is achieved by using a near-field microprobe (TeraSpike TD-800-X-HR, Protemics GmbH) for photo-conductive THz detection which is scanned across the investigated IBC cell in a distance of few tens of microns. The setup is schematically depicted in Fig. 2 (a), showing also a blow-up of the microprobe-tip.

The sheet resistance R_{sh} of a thin conductive layer on top of a substrate is calculated from the measured THz transmission amplitude reduction generated by the doping layer [9] using the Tinkham formula [10]:

$$\frac{1}{R_{sh}^{i}} = \frac{n+1}{Z_0}\left[\frac{E_{SL}^{ref}}{E_{SL}^{i}}\left(1+\frac{Z_0}{R_{sh}^{ref}(n+1)}\right)-1\right] \qquad (1)$$

E_{SL} represents the transmitted THz field amplitude through the sample with conductive layer. The superscript *i* indicates a position i(x,z) anywhere on the sample, while the superscript *ref* indicates a position on a reference area on the sample with known R_{sh}. Further constants are the substrate refractive index *n* and the free-space impedance Z_0. The method can also take into account a second conductive layer on the other side of the cell (e.g. an FFE) if either the sheet resistance of this layer or its behavior in respect to the rear R_{sh} is known.

3. THz mapping of interdigitated diffused structures

In order to show the advantages of THz transmission measurements, we compared two emitters used for the boron doped regions of IBC cells. The emitters were obtained with different boron diffusion recipes, and subsequent etching for R_{sh} tuning. First, we used a standard 4pp measurement (in a ShereScan device) to compare the two emitters. Figures 3(a-b) show 4pp R_{sh} maps of the emitters obtained with the two recipes. The maps were measured on the FFE of full-area IBC cells. The rear-side diffused IBC structures could be measured because of the limited 4pp resolution. From the maps it is clear that recipe 2 (b) improves the B diffusion homogeneity over the entire wafer with respect to recipe 1 (a). While recipe 2 looks very homogeneous over the entire wafer, it was not possible to measure R_{sh} up to the very edge of the wafer without distortions due to a distorted current path of the 4pp measurement. For this reason, the data points at the edge of the maps in Fig. 3a and 3b were measured 11 mm from the wafer edge.

Next, we used a THz tool to measure diffused IBC cells obtained with the two diffusion recipes. Before the THz measurement, the cells were stripped of the metal contact by means of wet etching in a H_3PO_4/HNO_3 solution. Since front and rear emitter are the same, we could measure fully diffused wafers and use the 2-layer approach. Figure

3(c) and (d) show R_{sh} maps of IBC cells with diffusion 1 and 2, respectively, measured with a THz tool. The R_{sh} maps clearly resolve the interdigitated fingers of the IBC cell (see also inset in fig. 3(f)). The areas with higher R_{sh} (warm colors) correspond to emitter fingers, while lower R_{sh} (cold colors) is measured on the BSF fingers. Note that for recipe 1 the THz R_{sh} map of the emitter part matches very closely the 4pp map on the unpatterned wafer, over the entire wafer area. However, the THz map of recipe 2 shows a non-uniform region very close (less than 2 cm) to the wafer edge. We have checked on a cleaved wafer that this is not an artefact of the measurement. Fig. 3(e) and (f) show line scans taken from the maps of (c) and (d), respectively. The boron diffusion recipe 1 creates large non-uniformities in R_{sh} in an area between 4 and 6 cm from the edge of the wafer. The R_{sh} at the very edge of the wafer reaches values up to 150 Ω/sq, compared to an R_{sh} of 72 Ω/sq at the centre of the wafer. Recipe 2, on the other hand, creates p^+ Si with a more uniform profile, with an R_{sh} of 85 Ω/sq over large part of the wafer. The R_{sh} however increases to 100 Ω/sq in proximity of the edge of the cell.

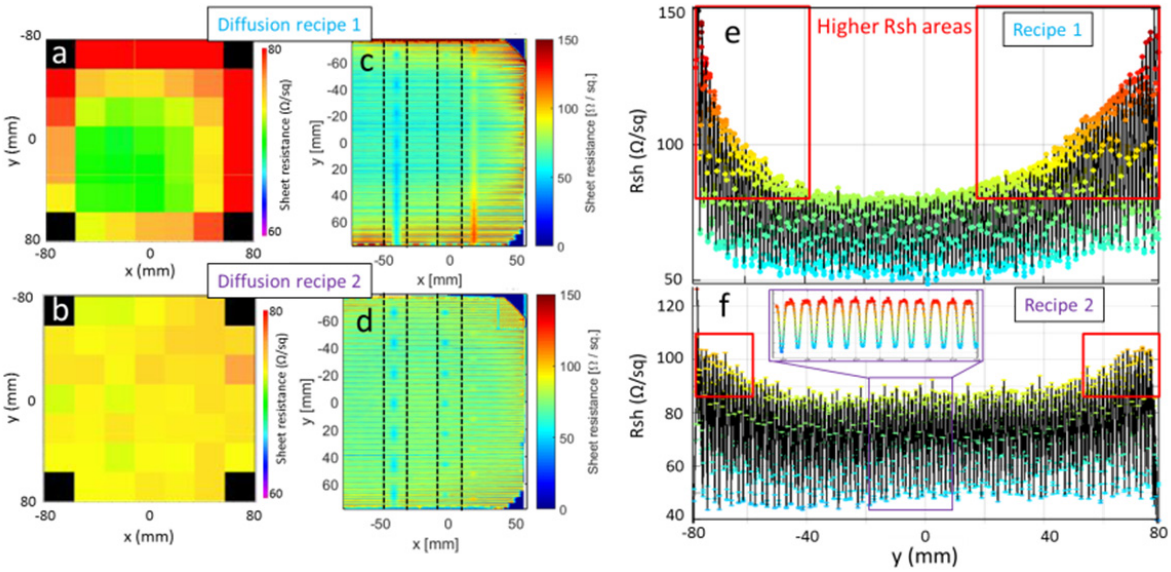

Fig. 3. (a-b) 4pp (Sherescan) maps of 2 diffusion recipes; (c-d) THz R_{sh} maps; (e-f) line scans from THz maps.

Overall, Figure 3 shows that THz maps introduce two main advantages over 4pp maps. First, the R_{sh} maps have a much higher resolution, which allows studying real IBC cell structures. They can be measured on cell half-fabricates, or on complete cells after stripping the rear-side metallization (this approach was used for the data in Fig. 2c and d). Second, R_{sh} can be measured up to the very edge of the wafer, and thus inhomogeneities can be detected much closer to the edge of the wafer. As we will show in the next paragraph, these inhomogeneity can have important effects on the cell performance, such as a lower V_{oc} due to higher metal contact region recombination.

Note that the THz transmission R_{sh} mapping measurement can also be done on metallized samples. Figure 4(a) shows a picture of the THz setup with a metallized IBC sample mounted for measurement. Figure 4(b) shows the measured THz map on the same sample. As can be seen, the emitter and BSF diffused fingers can be clearly resolved as well as the metallized parts, which appear as low R_{sh} values due to the fact that metals efficiently block the THz radiation.

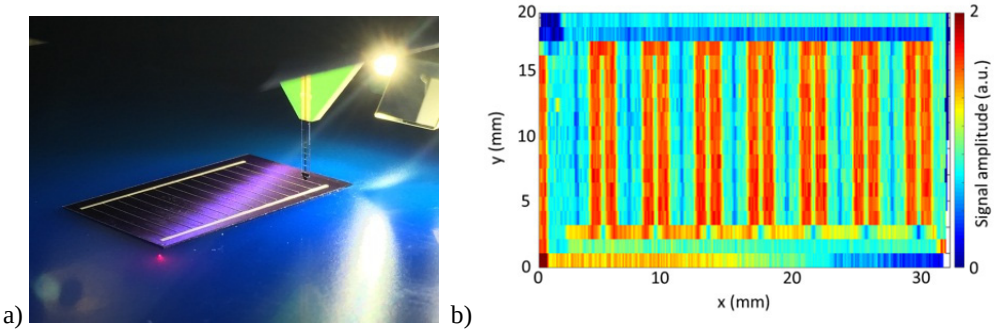

Fig. 4. (a) Photograph of the THz probe tip and metallized IBC sample. (b) THz transmission R_{sh} map of the sample shown in (a).

4. V_{oc} mapping method and edge effects

In order to study the effect of the higher R_{sh} at the edge of the wafer we developed a technique which allows mapping of the V_{oc} over the area of the cell using a SunsVoc tool. The IBC cell was illuminated at the rear side while the V_{oc} was measured by contacting 2 contact pads of different polarities with metal pins. We probed different pairs of contact pads, both at the centre as well as at the edge of the cell. Figure 5 (a) shows a map of the rear side of the Mercury IBC cell where the contacting points are shown as green and red dots, representing the two polarities. In total, 22 pairs of pads were measured, which are identified by the numbers (measurement ID) shown in Fig. 5(a). For each of these measurements, the V_{oc} and pFF were recorded. In this paper we focus on V_{oc} effects only.

Figure 3b shows the measured V_{oc} at the centre (measurement ID = 6-17) and at the edges of the completed IBC FFE cell (measurement ID = 1-5, 18-22). Results are shown for Diffusion 1 (blue) and Diffusion 2 (purple). First, we observe a 15 mV improvement in V_{oc} for recipe 2 with respect to recipe 1. It was shown before that this V_{oc} difference is largely due to rear-side pn-junction recombination in recipe 1, which is solved with recipe 2 and resulted in an absolute 1% gain in efficiency [2].

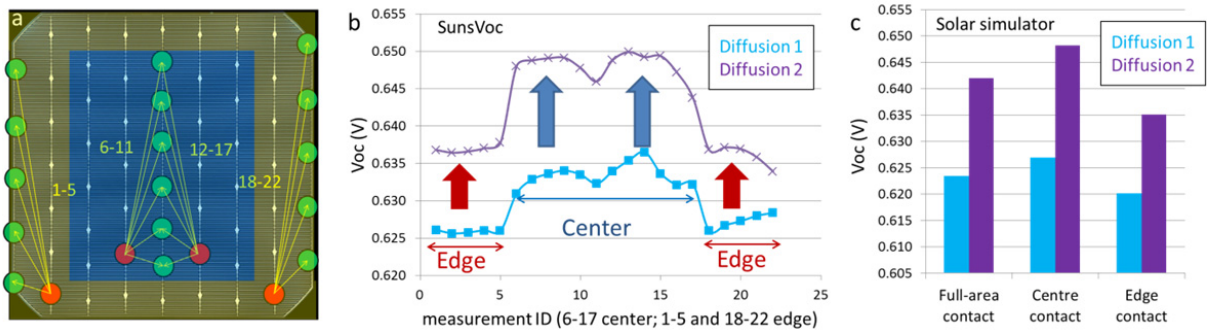

Fig. 5. (a) Map of the rear-side of a Mercury IBC cell. The green and red dots and the numbers indicate the contact points and measurement ID for the SunsVoc mapping method. The yellow and blue area indicate the contacted region for the local V_{oc} measurements in the solar simulator. (b) V_{oc} mapping data from the SunsVoc measurement. (c) V_{oc} data measured in the solar simulator.

While the overall V_{oc} is increased for recipe 2, we also note that the V_{oc} measured at the edge of the wafer is lower than that of the centre. For recipe 1, the V_{oc} variation between centre and edge is about 10 mV, but the overall V_{oc} level is low due to pn-junction recombination. For the better performing recipe 2 however, the edge V_{oc} drop is even more significant (17 mV). We have checked that the drop of V_{oc} at the edge is neither due to pn-junction recombination nor due to the presence of a FFE. Interestingly, the lower V_{oc} corresponds to the higher R_{sh} near the edge, which could only be observed with THz mapping.

In order to confirm the SunsVoc results (which could be influenced by the lamp homogeneity), we performed one Sun I-V measurements on different areas of the cells in a Wacom solar simulator. By isolating the area shown in blue (yellow) in Fig. 5 (a) we could measure the I-V parameters of the cell when only the edge (centre) region is contacted. The fully-contacted cell case was also measured for completeness. Figure 5(c) shows the V_{oc} as measured by one Sun I-V measurement. Data are shown for Diffusion 1 (blue) and 2 (purple). The V_{oc} variations between the edges and the centre measured in the SunsVoc are confirmed one Sun I-V measurements. Note that the full-area V_{oc} (first column) is lower than the V_{oc} measured at the centre (second column). A difference of 6 mV is found for the best performing recipe (purple color). Therefore, this analysis shows that by improving the V_{oc} at the edge there is a further potential gain in absolute efficiency of at least 0.2% (not considering FF and J_{SC} effects) for the best performing diffusion diffusion recipe.

The lower V_{oc} at the edges can be explained by the emitter doping variations which were identified with THz R_{sh} mapping. It is well known that the recombination prefactor for the metal contacts $J_{0,metal}$ is given by

$$J_{0,metal} \approx qD_{h/e} \int_0^{W-} \frac{n_{i,eff}^2}{N_{D/A}} dx$$

with q the elementary charge, $D_{h/e}$ the diffusion constant for electrons or holes, $N_{D/A}$ the doping level of donors or acceptors respectively, W^- the base side edge of the doped region and $n_{i,eff}$ the effective intrinsic carrier concentration. If the doping concentration is high (as shown by the schematics in Fig. 6(a)), the highly doped region near the contact effectively shields the minority carriers from the recombination active region of the metal. In regions where the doping is lower (which also results in the higher sheet resistance, see Fig. 6(b)), the charge carrier recombination at the metal contact is increased [11]. Assuming a similar etch depth (black vertical line) of the screen printed paste in the different regions of the cell, the higher doping concentration of the profile at the centre will yield a better screening effect and thus reduce contact recombination. This hypothesis thus explains well the V_{oc} variations observed on cell level between centre and edge.

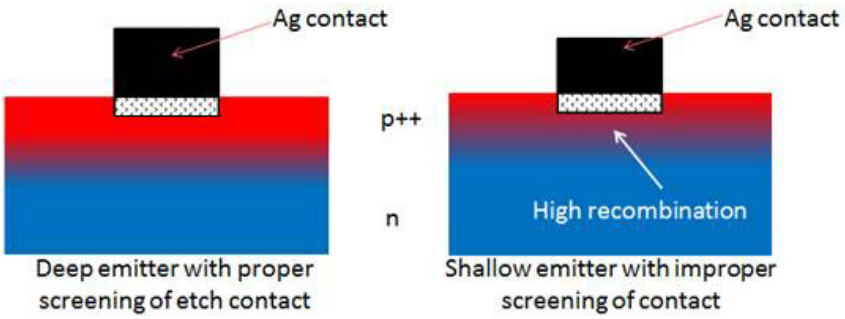

Fig. 6. Schematics of regions of the cell with high (left) and low (right) emitter doping, corresponding to regions of low and high R_{sh}, respectively.

5. Conclusion

We have presented a new method to make R_{sh} maps of solar cells with a much higher resolution than standard 4-point-probe methods. The new method is based on THz transmission through a doped wafer, and is particularly suited to measure R_{sh} of interdigitated diffusions, featuring small structures. Using THz transmission measurements we were able to unveil edge effects in industrial IBC cells which were not detectable before with standard 4pp measurements. The THz method allowed to detect more lightly doped edge regions which caused higher contact recombination and thus a lower V_{oc} at the edges. Improving the lower V_{oc} at the edges can result in a 0.2% absolute improvement of the cell efficiency. Therefore, we have shown that THz mapping is a powerful tool to optimize the cell process before a cell is made which reduces development effort and potentially production cost.

Acknowledgements

This work was supported by the Dutch Ministry of Economic Affairs, within the TKI framework, project IBChampion.

References

[1] Smith et al. SunPower's Maxeon Gen III solar cell: High Efficiency and Energy Yield", Proc. 39th IEEE PVSC, Tampa, 2013
[2] Hermle M, et al. Shading Effects in Back-Junction Back-Contacted Silicon Solar Cells. Proc. 33rd IEEE PVSC, San Diego, CA, 2008.
[3] Granek F, et al. ,"Enhanced lateral current transport via the front N+ diffused layer of n-type high-efficiency back-junction back-contact silicon solar cells", Prog. Photovolt: Res. Appl. 2009; V17(1):47-56
[4] Sah C, et al. Floating Emitter Solar Cell, US patent 4,665,277, 1987.
[5] Cesar I, Guillevin N, Burgers AR, Mewe AA, Koppes M, Anker J, Geerligs LJ, Weeber AW. Mercury: A back junction back contact front floating emitter cell with novel design for high efficiency and simplified processing. Energy Procedia.2014;55:633 – 42
[6] Romijn IG, et al. Industrial Cost Effective n-Pasha Solar Cells with >20% Cell Efficiency, Proc. 29th EU PVSEC, Amsterdam, 2014
[7] Nagel M, Safiei A, Sawallich S, Matheisen C, Pletzer TM, Mewe AA, van der Borg NJCM, Cesar I, and Kurz H. THz microprobe system for contact-free high-resolution sheet resistance imaging, Proc. 28th EU PVSEC 2012; 856-860
[8] Wächter M, Nagel M, and Kurz H. Tapered photoconductive terahertz field probe tip with subwavelength spatial resolution, Appl. Phys. Lett. 2009; 95(4):0411121
[9] Herrmann M, Tani M, Sakai K and Fukasawa R. Terahertz imaging of silicon wafers, J. of Appl. Phys. 2002; 91(3): 1247-1250
[10] Tinkham M. Energy Gap Interpretation of Experiments on Infrared Transmission through Superconducting Films, Phys. Rev. 1956; 104: 845-846
[11] Cuevas A, et al. Surface recombination velocity of highly doped n-type silicon, J. of Appl. Phys. 1996; 80(6):3370